Research Square

Preprints are preliminary reports that have not undergone peer review.
They should not be considered conclusive, used to inform clinical practice,
or referenced by the media as validated information.

Neural Control Model Personalizationusing an Improved Synergy Optimization Framework

Mohammad S. Shourijeh

mohammad.s.shourijeh@gmail.com

The University of Texas Health Science Center at Houston

Method Article

Keywords:

Posted Date: November 9th, 2026

DOI: https://doi.org/10.21203/rs.3.rs-11629049/v1

License: This work is licensed under a Creative Commons Attribution 4.0 International License.
Read Full License

Additional Declarations: No competing interests reported.

Neural Control Model Personalization using an Improved Synergy Optimization Framework

Mohammad S. Shourijeh

November 5, 2026

Abstract

Muscle synergy models reduce the underdetermined muscle activation search by representing activations with a small number of time-varying synergy commands and muscle-specific synergy vector weights. In the original Synergy Optimization (SynO) method, both variable blocks were solved simultaneously using nonlinear optimization, resulting in a computationally demanding neural control personalization problem. This study presents an updated implementation, termed SynOx, that alternates between nonnegative least-squares updates of synergy command nodes and synergy vectors while retaining activation bounds, joint moment tracking, and squared-activation minimization. In the benchmark runs, SynOx was over 100 times faster than the original SynO implementation while maintaining joint moment matching quality: fits using 2 through 6 synergies stopped after 3 to 6 alternating iterations, required 3.11 to 17.56 s, and reached joint moment qualities from 91.90% to 99.68%. Faster neural control personalization facilitates construction of personalized neuromusculoskeletal models for neurorehabilitation treatment design and optimization.

Introduction

Estimating muscle activations and forces from movement data remains underdetermined because the number of muscles in a musculoskeletal model exceeds the number of known joint moment equations at each time frame [1]. Static optimization resolves this redundancy by adding an objective, commonly the minimization of squared activations or muscle forces [2–4]. The low-effort objective is computationally convenient, but it tends to suppress antagonist coactivation and can therefore alter estimates of joint stiffness and neural control strategy during gait [5–7].

Dynamic optimization estimates muscle excitations over a movement while satisfying the equations of motion and muscle activation and contraction dynamics [8]. In EMG-driven modeling, processed EMG signals provide muscle-specific inputs to activation dynamics, and muscle forces are calculated from the resulting activations and muscle-tendon kinematics [9].

Muscle synergy models constrain the distribution of activation across muscles by expressing their activity as combinations of shared control signals. Time-varying synergy commands and time-invariant synergy vectors reconstruct the activation of each muscle [10–15]. Low-dimensional structure requires careful interpretation, since biomechanical constraints and task equations can

also produce apparent coordination [16–18]. Nonetheless, synergy constraints are useful not only for neural control model personalization but also for treatment design and optimization, because the resulting commands and vectors define a compact set of controls for movement simulations [19–23].

The original SynO formulation imposed a nonnegative muscle synergy structure on activations estimated by optimization and compared static optimization with SynO using 2 through 6 synergies [7]. Its design variables were the synergy command nodes and synergy vector weights, which coupled the entire gait cycle in one nonlinear constrained optimization. The formulation followed the algebraic structure of nonnegative matrix factorization (NMF), but simultaneous optimization of both variable blocks was computationally demanding. SynO was subsequently implemented as Neural Control Personalization (NCP) in the Neuromusculoskeletal Modeling (NMSM) Pipeline [23].

The present study tested whether alternating optimization of synergy command nodes and synergy vector weights could reduce the computational cost of SynO while preserving joint moment reconstruction. The resulting implementation, termed SynOx, updated synergy commands with synergy vectors fixed and then updated synergy vectors with synergy commands fixed. It combined joint moment tracking, activation bounds, nodal command parameterization, and squared-activation minimization with the iterative structure of NMF algorithms [24, 25]. Multiple NMF initializations limited dependence on a single initial factorization, and objective histories documented the stopping behavior [26]. More computationally efficient neural control personalization would facilitate construction of personalized models for subsequent treatment design and optimization in neurorehabilitation.

Methods

Experimental data and musculoskeletal model

Experimental walking data were collected from a 79-year-old man with chronic right-sided hemiparesis after stroke (height 1.70 m, mass 80.5 kg, lower-extremity Fugl-Meyer Motor Assessment 32/34). The University of Florida Health Science Center Institutional Review Board (IRB-01) and the Malcom Randall VA Medical Center Research and Development Committee approved data collection, and the participant provided written informed consent. Marker trajectories (Vicon), ground reactions (Bertec), and EMG signals (Motion Lab Systems) were recorded simultaneously during tied-belt treadmill walking at 0.5 and 0.8 m/s. Surface and fine-wire electrodes recorded 16 muscles per leg, including the adductor longus, iliopsoas, tibialis posterior, extensor digitorum longus, and flexor digitorum longus. Marker and ground reaction data were filtered with a fourth-order, zero-phase Butterworth filter at $7/t_f$ Hz, where t_f is gait-cycle duration. EMG signals were high-pass filtered at 40 Hz, demeaned, rectified, and low-pass filtered at $3.5/t_f$ Hz; each envelope was normalized to its maximum across walking cycles and offset to a zero minimum. Trajectories were resampled to 101 time points, with 200 ms of preceding EMG retained for electromechanical

delay [27].

A full-body musculoskeletal model was scaled from a static standing trial, and lower-limb joint and muscle-tendon parameters were personalized. Knee and ankle parameters were adjusted to reduce marker errors; hip parameters were retained to preserve anatomical muscle paths, and subtalar parameters were retained because the available motion was insufficient for their identification. Muscle-tendon personalization fitted inverse-dynamics joint moments, adjusted muscle-tendon and activation-dynamics parameters, and estimated activation signals for muscles without recorded EMG. The present analysis used the resulting right-leg model with 45 muscles and six joint coordinates. Joint moments and muscle-tendon parameters from the personalized EMG-driven model supplied the targets and force calculations for one gait cycle. The complete activation reference therefore included model-derived estimates as well as trajectories informed by the recorded EMG.

At normalized gait time t, tendon force for muscle i following a rigid-tendon formulation was represented as

$$F_i^T(t) = (a_i(t)F_i^{\text{act}}(t) + F_i^{\text{pas}}(t))F_{max,i}, \tag{1}$$

where a_i is muscle activation, $F_{max,i}$ is muscle maximum isometric force parameter, and $F_i^{\text{act}}(t)$ and $F_i^{\text{pas}}(t)$ are dimensionless muscle active and passive force functions, respectively, normalized to $F_{max,i}$ [1]. The active function accounts for the force-length and force-velocity effects, whereas the passive function accounts for passive force arising from muscle-tendon length. The model-generated joint moment for coordinate j was

$$M_j(t) = \sum_{i=1}^{N_m} r_{ji}(t)F_i^T(t), \tag{2}$$

where r_{ji} is the moment arm of muscle i about coordinate j. At prescribed kinematics, Eqs. 1 and 2 are linear with respect to muscle activation.

Original SynO structure

The original SynO formulation [7] constructed activation for muscle i from n synergy commands and synergy vectors,

$$a_i(t) = \sum_{p=1}^{n} V_{ip}C_p(t), \qquad V_{ip} \geq 0, \quad C_p(t) \geq 0, \tag{3}$$

where V_{ip} is the contribution of synergy vector p to muscle i, and $C_p(t)$ is its time-varying synergy command. The terms synergy commands and synergy vectors follow the terminology recommended by Sharif Razavian and colleagues [28]. The original SynO implementation parameterized each command using interpolation nodes,

$$C_p(t) = \sum_{\ell=1}^{N_b} B_\ell(t)c_{\ell p}, \qquad N_b = 21, \tag{4}$$

where $B_\ell(t)$ is the interpolation basis value for node ℓ at time sample t, and $c_{\ell p}$ is a design variable defining that node. In this nonlinear formulation used by the original SynO method, the synergy command nodes $c_{\ell p}$ and synergy vector weights V_{ip} were optimized simultaneously while matching joint moments and penalizing activation magnitude [7].

SynOx formulation

SynOx used Eqs. 3 and 4 and solved for the nonnegative synergy command nodes $c_{\ell p}$ and synergy vector weights V_{ip} by block alternation. Muscle activations were constrained to $0 \leq a_i(t) \leq 1$. After each update, every synergy vector was normalized to unit L_2 norm and the reciprocal scale was applied to its command nodes. This step removed the arbitrary scale exchange between $\mathbf{C}$ and $\mathbf{V}$ without changing the reconstructed activations. The original SynO implementation used unit-sum normalization for the same purpose [7].

For a selected number of synergies n, the objective is written in discrete form as

$$J\big|_{\{c_{\ell p}\},\{V_{ip}\}} = \frac{1}{N_t N_j} \sum_{k=1}^{N_t} \sum_{j=1}^{N_j} \left[\frac{M_{jk} - M^{\star}_{jk}}{\sigma_M} \right]^2 + \frac{1}{N_t N_m} \sum_{k=1}^{N_t} \sum_{i=1}^{N_m} \left(\frac{a_{ik}}{\sigma_a} \right)^2, \tag{5}$$

where $M^{\star}_{jk}$ is the EMG-driven target joint moment, M_{jk} is the joint moment calculated from Eqs. 1 and 2, and $a_{ik} = \sum_{p=1}^{n} V_{ip} C_{pk}$, with $C_{pk} = C_p(t_k)$. The maximum allowable errors were $\sigma_M = 1$ N m for joint moments and $\sigma_a = 0.05$ for normalized muscle activation. The activation value matched the default NMSM Pipeline setting [29]. These allowable-error values scaled the objective terms; they were not hard constraints on individual residuals. Each sum was divided by its number of time samples and joint coordinates or modeled muscles.

When an activation target from the EMG-driven model was available, its tracking residual replaced activation minimization for that muscle; activation was minimized for muscles without a target. Here, available EMG activations refer to the 45 activation trajectories from the EMG-driven model, including estimates for muscles without recorded EMG. The Supplementary Material compares the six-synergy joint-moment-only fit with a fit tracking joint moments together with all 45 EMG-driven activations. The formulation also accommodates a subset of available activation targets.

Alternating solver

At alternating iteration q, the solver first solved for the synergy command nodes $\mathbf{c}$ while holding the synergy vectors $\mathbf{V}$ fixed. It then updated the synergy vectors with those command nodes fixed. The conditional least-squares problems produced trial updates,

$$\begin{aligned} \mathbf{c}^{(q+1)}_{\text{trial}} &= \arg\min_{\mathbf{c} \geq 0} \; J\big|_{\mathbf{c},\, \mathbf{V}=\mathbf{V}^{(q)}}, \\ \mathbf{V}^{(q+1)}_{\text{trial}} &\approx \arg\min_{\mathbf{V} \geq 0} \; J\big|_{\mathbf{c}=\mathbf{c}^{(q+1)}_{\text{trial}},\, \mathbf{V}}. \end{aligned} \tag{6}$$

Activation and predicted joint moment were linear in one variable block when the other block was fixed. All command nodes were updated together. For computational efficiency, the synergy-vector problem was approximated through one sequential pass over muscles, solving the nonnegative weights for each muscle while holding the remaining muscle weights fixed. The approximation symbol distinguishes this pass from a complete joint solution for all synergy vector weights. Each muscle update used the current joint moment residual. For the command update, each predicted activation was evaluated as

$$a_i(t) = \sum_{p=1}^{n} V_{ip}^{(q)} \sum_{\ell=1}^{N_b} B_\ell(t) c_{\ell p}. \tag{7}$$

For the synergy-vector update, each predicted activation was evaluated as

$$a_i(t) = \sum_{p=1}^{n} V_{ip}\, C_{p,\mathrm{trial}}^{(q+1)}(t). \tag{8}$$

Substitution of these expressions into Eqs. 1, 2, and 5 produced the two least-squares updates. The nonnegative least-squares solves used MATLAB's active-set algorithm with its default input-scaled tolerance.

After both block updates, the complete objective was evaluated. A damped candidate was tested using

$$(\mathbf{c}_\alpha, \mathbf{V}_\alpha) = (1-\alpha)(\mathbf{c}^{(q)}, \mathbf{V}^{(q)}) + \alpha(\mathbf{c}_{\mathrm{trial}}^{(q+1)}, \mathbf{V}_{\mathrm{trial}}^{(q+1)}), \tag{9}$$

where $\alpha \in \{1, 0.5, 0.25, 0.125, 0.0625, 0\}$. The largest step that did not increase the objective was accepted. The nonnegative least-squares updates did not impose the upper activation bound internally; scaling of commands or muscle weights enforced that bound afterward. This scaling could increase the objective relative to the least-squares solution, so the backtracking test evaluated each candidate after bound enforcement. Reciprocal normalization of synergy vectors and commands preserved their activation product and did not itself change the objective.

Initialization and solver settings

An initial activation history was estimated one time sample at a time by matching the target joint moments, enforcing $0 \le a_i \le 1$, and applying a small continuity penalty relative to the preceding sample. This activation history was factorized with MATLAB's alternating-least-squares NMF algorithm using 3 independent initializations and a maximum of 100 NMF iterations [30]. The resulting synergy commands and synergy vectors initialized the proposed alternating optimization. The primary analysis then changed only the number of synergies, $n = 2, 3, 4, 5, 6$. Table 1 lists the settings that directly governed the optimization and its stopping criterion.

For the runtime benchmarks, joint moment residuals were normalized by the root-mean-square target joint moment, and the sum of squared activations had a coefficient of 10^{-4}. Figure 3 reports this solver objective, which uses different relative weighting from the allowable-error-normalized criterion in Eq. 5. The costs in Table 2 were obtained by evaluating Eq. 5 at the resulting fitted

Table 1: Primary SynOx solver settings and allowable errors.

Setting	Value
Model dimensions	45 muscles, 6 joint coordinates, 101 time samples
Synergy counts	2, 3, 4, 5, and 6
Command parameterization	21 nodes per synergy; shape-preserving cubic interpolation
Activation bounds	$0 \leq a_i(t) \leq 1$
Allowable errors	$\sigma_M = 1$ N m; $\sigma_a = 0.05$
Maximum alternating iterations	100
Convergence tolerance	10^{-6} relative objective improvement
NMF initialization	Alternating least squares; 3 initializations; 100 iterations

solutions.

Outcome measures

Joint moment matching quality was reported as

$$\mathrm{Q_M} = 100 \left(1 - \frac{\sum_{k=1}^{N_t} \sum_{j=1}^{N_j} [M_{jk} - M_{jk}^{\star}]^2}{\sum_{k=1}^{N_t} \sum_{j=1}^{N_j} (M_{jk}^{\star})^2} \right). \tag{10}$$

Similarly, activation quality Q_a, when reported, used the same expression with activation from the EMG-driven model as the reference.

Original SynO was run with two through six synergies using MATLAB's `fmincon`, with and without parallelization while SynOx used no parallelization. The two SynO configurations served as computational-time references for SynOx. Benchmarks used Windows 10, an Intel Core i7-6700HQ CPU at 2.60 GHz, and 32 GB of RAM. Runtimes were means of three runs. SynOx timing included basis construction, NMF initialization, alternating updates, and the final command refinement, and excluded data loading, plotting, and file output.

Results

Joint moment quality increased from 91.90% with two synergies to 99.68% with six synergies. The corresponding original SynO qualities were 92.01%, 98.11%, 98.79%, 99.65%, and 99.73% for two through six synergies (Table 2). SynOx stopped after 3 to 6 alternating iterations. Its runtime increased from 3.11 to 17.56 s, compared with 350 to 3060 s for parallel SynO and 460 to 3630 s for nonparallel SynO.

Table 2: Joint moment quality and runtime benchmarks for SynOx and original SynO. Original SynO runtimes are means of three runs. SynOx used no parallelization; par. denotes parallelization. Costs are evaluations of Eq. 5 at the fitted SynOx solutions.

	Q_M (%)				Runtime (s)		
Synergies	SynOx	SynO	J	Iters	SynOx	SynO, par.	SynO, no par.
2	91.90	92.01	86.08	4	3.11	350	460
3	98.10	98.11	41.46	4	4.67	680	910
4	98.77	98.79	26.14	3	5.06	1800	2170
5	99.63	99.65	26.51	4	8.88	2330	2930
6	99.68	99.73	30.01	6	17.56	3060	3630

Discussion

Neural control model personalization estimates how muscle activity generates an individual's movement, a prerequisite for using neuromusculoskeletal simulations to evaluate rehabilitation treatments. SynO and its subsequent NCP implementation in the NMSM Pipeline address this task, but simultaneous optimization of synergy commands and synergy vectors is computationally demanding [7, 23]. We proposed SynOx to reduce that computational burden. Like the original SynO method, SynOx constrains muscle activations to a low-dimensional, nonnegative synergy representation. The principal change is computational. Alternating synergy command updates with synergy vector updates replaces the coupled nonlinear optimization with a sequence of nonnegative least-squares problems. This block-wise principle is shared with alternating NMF, although the overall optimization remains bilinear and nonconvex [12, 24, 25].

SynOx maintained the joint moment matching quality of SynO. Across two through six synergies, the difference between the methods was at most 0.11 percentage points, with the six-synergy estimates reaching 99.68% for SynOx and 99.73% for SynO. Additional synergies progressively reduced reconstruction error, but agreement with joint moments did not establish equivalence of the underlying muscle activations.

SynOx was over 100 times faster than the original SynO implementation in every benchmark, despite using no parallelization. Table 2 corresponds to speedups of approximately 113–356 times relative to parallel SynO and 148–429 times relative to nonparallel SynO. For six synergies, SynOx required 17.56 s, compared with 3060 s and 3630 s for the two SynO configurations. Alternating small conditional problems reduced the need for a general nonlinear optimizer to adjust both synergy variable blocks simultaneously.

The squared-activation term addresses the remaining underdetermination when only joint moments are tracked. Many distributions of muscle activity can produce similar net joint moments. Activation minimization discourages large activations that are not required for joint moment reconstruction, while the synergy representation restricts which distributions are possible.

Available activations from EMG measurements or the EMG-driven model supply additional information about the distribution of muscle activity. Tracking these activations replaces the low-effort preference with agreement to muscle-specific targets. The supplementary combined fit used

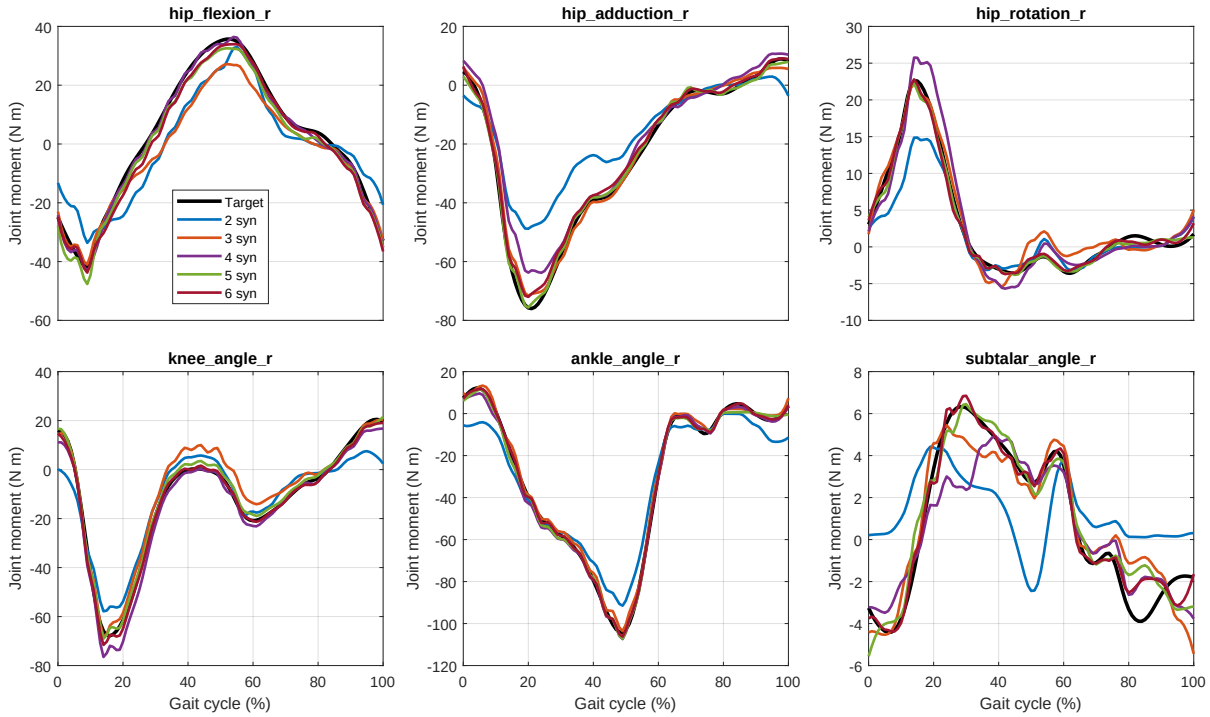


Figure 1: Joint moments (N m) over one normalized gait cycle for SynOx with 2 through 6 synergies. Each panel plots one joint coordinate. Black denotes the EMG-driven target joint moment. Blue, orange, purple, green, and red denote estimates using 2, 3, 4, 5, and 6 synergies, respectively. Only the bottom row shows gait-cycle ticks and labels.

all 45 EMG-driven activation trajectories, so it did not require a separate activation-minimization term. With partial availability, the combined formulation tracks the available targets and minimizes activation for muscles without targets. It follows the NCP use of activation estimates obtained from the muscle-tendon personalization (MTP) tool [23].

A compact synergy representation should not be interpreted as proof that its components identify neural modules. Biomechanical and task constraints can create low-dimensional structure even without an underlying modular neural controller [16, 18]. SynOx uses this representation as a computational constraint. Whether the resulting commands and vectors predict a response to treatment requires testing on movements or interventions that were not used for personalization. Accurate reconstruction of the fitted movement cannot establish that predictive validity.

The analysis used data from one participant, so its runtime and reconstruction quality do not characterize between-subject performance. NMF factorizations can depend on initialization and admit equivalent component orderings and scales [26]. Sensitivity to alternative initializations was not quantified. In addition, the activation and joint moment references came from the same EMG-driven model; agreement with these targets in the supplementary combined fit was therefore an internal consistency test, not an independent validation of estimated muscle activity. The runtime comparison evaluated original SynO, not the complete NCP implementation.

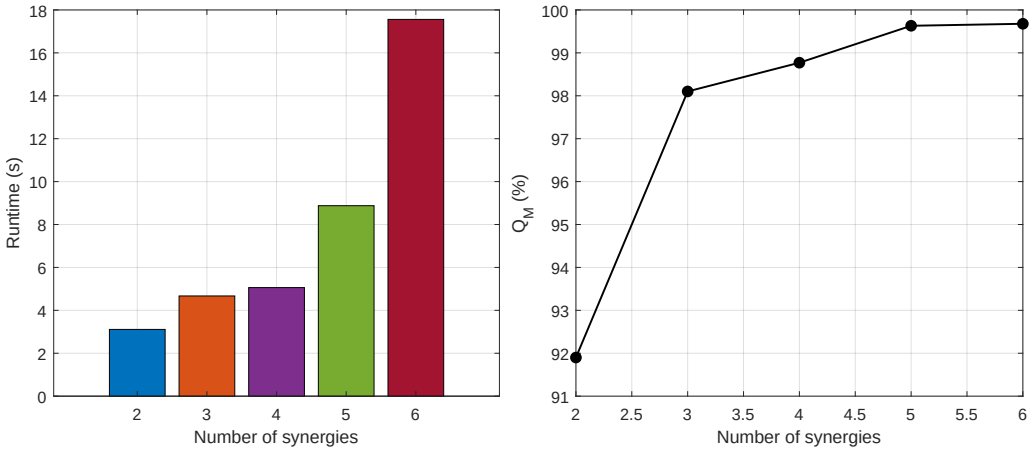


Figure 2: Runtime (s) and joint moment quality (%) for SynOx with 2 through 6 synergies for one gait cycle. Bar colors follow the 2-through-6-synergy color order in Fig. 1.

Conclusion

We proposed an improved approach for neural control model personalization through muscle synergies, named SynOx. The benchmarks were over 100 times faster than the original SynO method [7], which underlies NCP in the NMSM Pipeline [23], while preserving joint moment matching quality. More efficient neural control personalization can facilitate construction of personalized neuromusculoskeletal models for neurorehabilitation treatment design and optimization.

Ethics Approval and Consent to Participate

This study involved a secondary analysis of previously published experimental data. Original data collection and ethical approval were obtained by the primary investigators from the University of Florida Health Science Center Institutional Review Board (IRB-01) and the Malcom Randall VA Medical Center Research and Development Committee, with written informed consent provided by the participant.

Consent for Publication

Not applicable (secondary analysis of previously published data).

Availability of Data and Materials

The data utilized in this study are derived from previously published sources. Custom analysis code and implementation data will be available upon request.

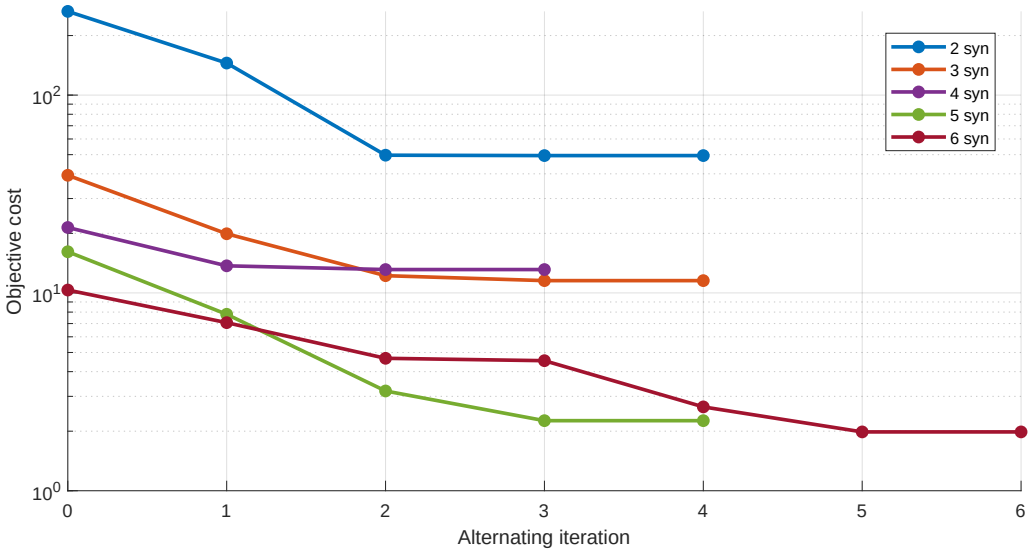


Figure 3: Solver cost histories for SynOx with 2 through 6 synergies for one gait cycle. Lines and circles identify accepted alternating iterations; iteration zero is the initial solution. Costs use the solver normalization described in Methods. Colors follow Fig. 1.

Competing Interests

The author has no competing interests to declare.

Funding

No funding was received for this work.

Authors' Contributions

M.S.S. conceived and designed the study, developed the code, performed testing and validation, and wrote the manuscript.

Acknowledgment

I thank B.J. Fregly for initial discussion around ways of improving synergy optimization and in general around model personalization.

References

[1] Felix E. Zajac. Muscle and tendon: Properties, models, scaling, and application to biomechanics and motor control. *CRC Critical Reviews in Biomedical Engineering*, 19(4):359–411, 1989.

[2] Roy D. Crowninshield and Richard A. Brand. A physiologically based criterion of muscle force prediction in locomotion. *Journal of Biomechanics*, 14:793–801, 1981. doi: 10.1016/0021-9290(81)90035-X.

[3] Riender Happee and Frans C. T. Van der Helm. The control of shoulder muscles during goal directed movements, an inverse dynamic analysis. *Journal of Biomechanics*, 28(10):1179–1191, 1995. doi: 10.1016/0021-9290(94)00181-3.

[4] Mohammad S Shourijeh, Naser Mehrabi, and John McPhee. Forward static optimization in dynamic simulation of human musculoskeletal systems: a proof-of-concept study. *Journal of Computational and Nonlinear Dynamics*, 12(5):051005, 2017.

[5] Etienne Burdet, Rieko Osu, David W. Franklin, Theodore E. Milner, and Mitsuo Kawato. The central nervous system stabilizes unstable dynamics by learning optimal impedance. *Nature*, 414:446–449, 2001. doi: 10.1038/35106566.

[6] David W. Franklin, Uta So, Mitsuo Kawato, and Theodore E. Milner. Impedance control balances stability with metabolically costly muscle activation. *Journal of Neurophysiology*, 92(5):3097–3105, 2004. doi: 10.1152/jn.00364.2004.

[7] Mohammad S. Shourijeh and Benjamin J. Fregly. Muscle synergies modify optimization estimates of joint stiffness during walking. *Journal of Biomechanical Engineering*, 142(1):011011, 2020. doi: 10.1115/1.4044310.

[8] Mark Ackermann and Antonie J. Van Den Bogert. Optimality principles for model-based prediction of human gait. *Journal of Biomechanics*, 43:1055–1060, 2010. doi: 10.1016/j.jbiomech.2009.12.012.

[9] David G. Lloyd and Thor F. Besier. An emg-driven musculoskeletal model to estimate muscle forces and knee joint moments in vivo. *Journal of Biomechanics*, 36(6):765–776, 2003.

[10] Lena H. Ting and Jane M. Macpherson. A limited set of muscle synergies for force control during a postural task. *Journal of Neurophysiology*, 93(1):609–613, 2005. doi: 10.1152/jn.00681.2004.

[11] Yuri P. Ivanenko, Richard E. Poppele, and Francesco Lacquaniti. Five basic muscle activation patterns account for muscle activity during human locomotion. *Journal of Physiology*, 556(1):267–282, 2004. doi: 10.1113/jphysiol.2003.057174.

[12] Matthew C. Tresch, Vincent C. K. Cheung, and Andrea d'Avella. Matrix factorization algorithms for the identification of muscle synergies: Evaluation on simulated and experimental data sets. *Journal of Neurophysiology*, 95(4):2199–2212, 2006.

[13] Guadalupe Torres-Oviedo, John M. Macpherson, and Lena H. Ting. Muscle synergy organization is robust across a variety of postural perturbations. *Journal of Neurophysiology*, 96: 1530–1546, 2006.

[14] Germana Cappellini, Yuri P. Ivanenko, Richard E. Poppele, and Francesco Lacquaniti. Motor patterns in human walking and running. *Journal of Neurophysiology*, 95(6):3426–3437, 2006. doi: 10.1152/jn.00081.2006.

[15] Emilio Bizzi and Vincent C. K. Cheung. The neural origin of muscle synergies. *Frontiers in Computational Neuroscience*, 7:51, 2013. doi: 10.3389/fncom.2013.00051.

[16] Katherine M. Steele, Matthew C. Tresch, and Eric J. Perreault. Consequences of biomechanically constrained tasks in the design and interpretation of synergy analyses. *Journal of Neurophysiology*, 2015. doi: 10.1152/jn.00769.2013.

[17] Matthew C. Tresch and Amy Jarc. The case for and against muscle synergies. *Current Opinion in Neurobiology*, 19:601–607, 2009.

[18] Jason J. Kutch and Francisco J. Valero-Cuevas. Challenges and new approaches to proving the existence of muscle synergies of neural origin. *PLoS Computational Biology*, 8:e1002434, 2012.

[19] Massimo Sartori, Leonardo Gizzi, David G. Lloyd, and Dario Farina. A musculoskeletal model of human locomotion driven by a low dimensional set of impulsive excitation primitives. *Frontiers in Computational Neuroscience*, 7:79, 2013. doi: 10.3389/fncom.2013.00079.

[20] Jason P. Walter, Allison L. Kinney, Scott A. Banks, Darryl D. D'Lima, Thor F. Besier, David G. Lloyd, and Benjamin J. Fregly. Muscle synergies may improve optimization prediction of knee contact forces during walking. *Journal of Biomechanical Engineering*, 136: 021031, 2014. doi: 10.1115/1.4026428.

[21] Benjamin R. Shuman, Marije Goudriaan, Kaat Desloovere, Michael H. Schwartz, and Katherine M. Steele. Muscle synergy constraints do not improve estimates of muscle activity from static optimization during gait for unimpaired children or children with cerebral palsy. *Frontiers in Neurorobotics*, 13:102, 2019. doi: 10.3389/fnbot.2019.00102.

[22] Nicholas A. Bianco, Carol Patten, and Benjamin J. Fregly. Can measured synergy excitations accurately construct unmeasured muscle excitations? *Journal of Biomechanical Engineering*, 140(1):011011, 2018. doi: 10.1115/1.4038199.

[23] Claire V. Hammond, Spencer T. Williams, Marleny M. Vega, Di Ao, Geng Li, Robert M. Salati, Kayla M. Pariser, Mohammad S. Shourijeh, Ayman W. Habib, Carol Patten, and Benjamin J. Fregly. The neuromusculoskeletal modeling pipeline: Matlab-based model personalization and treatment optimization functionality for opensim. *Journal of NeuroEngineering and Rehabilitation*, 22:112, 2025. doi: 10.1186/s12984-025-01629-5.

[24] Daniel D. Lee and H. Sebastian Seung. Learning the parts of objects by non-negative matrix factorization. *Nature*, 401(6755):788–791, 1999. doi: 10.1038/44565.

[25] Daniel D. Lee and H. Sebastian Seung. Algorithms for non-negative matrix factorization. In *Advances in Neural Information Processing Systems*, volume 13, pages 556–562, 2000.

[26] Mohammad S. Shourijeh, Teresa E. Flaxman, and Daniel L. Benoit. An approach for improving repeatability and reliability of non-negative matrix factorization for muscle synergy analysis. *Journal of Electromyography and Kinesiology*, 26:36–43, 2016. doi: 10.1016/j.jelekin.2015.12.001.

[27] Andrew J. Meyer, Ilan Eskinazi, Jennifer N. Jackson, Anil V. Rao, Carolynn Patten, and Benjamin J. Fregly. Muscle synergies facilitate computational prediction of subject-specific walking motions. *Frontiers in Bioengineering and Biotechnology*, 4:77, 2016. doi: 10.3389/fbioe.2016.00077.

[28] Reza Sharif Razavian, Gerard E. Francisco, and Mohammad S. Shourijeh. Muscle synergy: Definition, methods, applications, and future directions. SSRN preprint, August 18, 2026, 2026.

[29] RCNL. NMSM Pipeline: Neuromusculoskeletal modeling pipeline, 2024. URL `https://github.com/rcnl-org/nmsm-core`. GitHub repository.

[30] The MathWorks Inc. *MATLAB version R2023b*. The MathWorks Inc., Natick, Massachusetts, 2023.

Supplementary Files

This is a list of supplementary files associated with this preprint. Click to download.

- supp.zip